JACS
JOURNAL OF THE AMERICAN CHEMICAL SOCIETY
Article
pubs.acs.org/JACS

Design of Pd/PANI/Pd Sandwich-Structured Nanotube Array Catalysts with Special Shape Effects and Synergistic Effects for Ethanol Electrooxidation

An-Liang Wang, Han Xu, Jin-Xian Feng, Liang-Xin Ding, Ye-Xiang Tong, and Gao-Ren Li*

MOE Laboratory of Bioinorganic and Synthetic Chemistry, KLGHEI of Environment and Energy Chemistry, School of Chemistry and Chemical Engineering, Sun Yat-sen University, Guangzhou 510275, China

Supporting Information

ABSTRACT: Low cost, high activity, and long-term durability are the main requirements for commercializing fuel cell electrocatalysts. Despite tremendous efforts, developing non-Pt anode electrocatalysts with high activity and long-term durability at low cost remains a significant technical challenge. Here we report a new type of hybrid Pd/PANI/Pd sandwich-structured nanotube array (SNTA) to exploit shape effects and synergistic effects of Pd-PANI composites for the oxidation of small organic molecules for direct alcohol fuel cells. These synthesized Pd/PANI/Pd SNTAs exhibit significantly improved electrocatalytic activity and durability compared with Pd NTAs and commercial Pd/C catalysts. The unique SNTAs provide fast transport and short diffusion paths for electroactive species and high utilization rate of catalysts. Besides the merits of nanotube arrays, the improved electrocatalytic activity and durability are especially attributed to the special Pd/PANI/Pd sandwich-like nanostructures, which results in electron delocalization between Pd d orbitals and PANI π-conjugated ligands and in electron transfer from Pd to PANI.

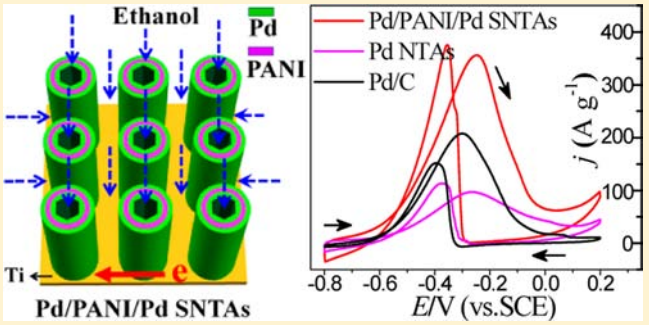

1. INTRODUCTION

It has been well-known that Pt is the best catalyst for fuel cells that are ideal for portable application.[1−4] However, the use of Pt catalysts is severely limited because of its high cost and limited resources.[5−11] So it is desirable to find new low-cost catalysts with high performance to replace the expensive and scarce Pt.[12−15] Recently, Pd has aroused increasing interest because of its greater abundance in nature and lower cost than Pt, and its outstanding electrocatalytic activity toward the oxygen reduction reactions for proton exchange membrane fuel cells (PEMFCs), especially toward the oxidation of small organic molecules for direct alcohol fuel cells (DAFCs).[16−30]

In addition, durability is another main challenge for commercializing electrocatalysts for fuel cells,[31−34] and it faces the following major problems: First, the electrocatalyst surface is usually heavily poisoned by strong adsorption of CO intermediates produced during fuel cell operation, thus lowering the activity and durability.[35−37] Second, the nanoparticles of catalysts are easily aggregated because of the drive of surface-energy minimization, leading to the low-electroactivity surface area and durability.[38−41] Third, at present, the most common supports for electrocatalysts are carbon materials,[42−44] which are vulnerable to corrosion/oxidation at high potentials (>0.7 V vs NHE) under the normal operating condition, resulting in poor durability of electrocatalysts because of the dissolution, Ostwald ripening, and aggregation.[45,46] The low polarity and high hydrophobicity features of carbon are also identified as major drawbacks to limit rate performance of carbon-supported catalysts. To resolve these problems, a number of strategies have been proposed, such as forming multimetallic Pt alloys,[5] depositing Pt on oxides,[46] and obtaining ultrathin Pt, Pd, and PtPd nanowires.[16,47,48] However, at present, no effective solution exists for addressing all of the above problems simultaneously.

Based on the above considerations, here we devote our attention to design and synthesize Pd-PANI composite electrocatalysts for DAFCs. For composite catalysts, it has been fully recognized that the shape effects and synergistic effects played a significant role in the catalytic activity and durability.[49−51] Recently, conducting polymer, especially polyaniline (PANI), as supports have received much attention for electrocatalysts because of their high chemical and electrochemical stability, high conductivity, ease of synthesis, benign environmental effect, good adhesion, and higher hydrophilic property than carbon materials.[52−57] PANI as supports can significantly improve the dispersion of noble metal and the ability of CO antipoisoning.[58,59] It also has been reported that nanotube arrays have attracted special interest because of the hollow and open structures, large specific surface areas, and anisotropic morphologies, which can obviously improve mass transport and catalyst utilization, and they are

Received: March 28, 2013
Published: July 9, 2013

   dx.doi.org/10.1021/ja403101r | J. Am. Chem. Soc. 2013, 135, 10703−10709

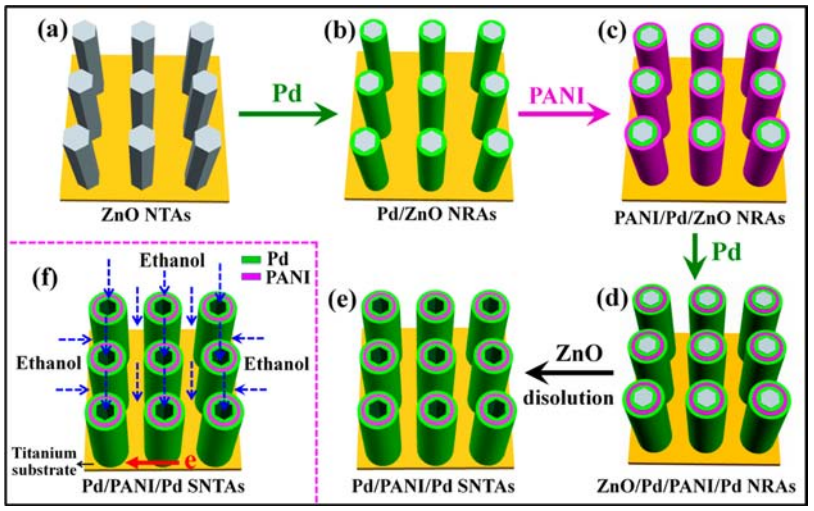

Figure 1. (a–e) Schematic illustration for the fabrication of Pd/PANI/Pd SNTAs. (f) Schematic illustration for the advantages of Pd/PANI/Pd SNTAs as a catalyst, such as large surface area, large open space, fast transport of active species, and rapid electron transmission.

much less vulnerable to dissolution, Ostwald ripening, and aggregation during fuel cell operation than the nanoparticles. However, up to now, it is still a huge challenge to realize the fabrication of orderly Pd-PANI composite nanotube arrays because of the difficulties involved in controlling the nucleation and growth of nanostructures in the presence of different precursors with various reduction kinetics.[60] Here we first design and synthesize Pd/PANI/Pd sandwich-structured nanotube arrays (SNTAs) to exploit the shape effects and synergistic effects for ethanol electrooxidation for DAFCs. The aligned SNTAs structure represents a novel prime example of catalysts with well-defined nanotube array structure, and they can provide large surface area, high utilization rate, and fast electrolyte penetration/diffusion. Besides the strong points of nanotube arrays, the Pd/PANI/Pd SNTAs also allow for strong synergistic coupling between inorganic Pd and organic PANI, which results in electron delocalization between Pd d orbitals and PANI π-conjugated ligands and in electron transfer from Pd to PANI. Herein, the electrochemical measurements show these fabricated Pd/PANI/Pd SNTAs exhibit high electrocatalytic activity and long-term durability and they show promising catalysts for DAFCs.

2. EXPERIMENTAL SECTION

Synthesis of Pd/PANI/Pd Sandwich-Structured Nanotube Arrays (SNTAs). $Zn(NO_3)_2{\cdot}6H_2O$ (99.99%, w/w), $PdCl_2$ (99.5%, w/w), and aniline (99.5%, w/w) were commercially available from Aladdin Chemistry Co. Ltd. NH_4NO_3 (99%, w/w), Na_2SO_4 (99%, w/w), and $C_6H_5Na_3O_7{\cdot}2H_2O$ (99%, w/w) were commercially available from Guangzhou Chemical Reagent Co. Ltd. Nafion (5 wt %) was commercially available from Sigma-Aldrich. All chemical reagents were all used as received. Electrodeposition was carried out in a simple three-electrode electrolytic cell via galvanostatic method, and a graphite electrode was used as the counter electrode (spectral grade, 1.8 cm^2). The details of the fabrication of Pd/PANI/Pd SNTAs are described as follows:

(1) ZnO nanorod arrays (NRAs) template was electrodeposited in a solution of 0.01 M $Zn(NO_3)_2$ + 0.05 M NH_4NO_3 with current density of 1.0 $mA{\cdot}cm^{-2}$ at 70 °C for 90 min. Ti plates (99.99%, 1.0 cm^2) were used as the substrates for electrodeposition, and they are prepared complying the following steps before each experiment: first polished by SiC abrasive paper from 300 to 800 grits, then dipped in HCl solution (5%) for 10 min and rinsed with acetone in ultrasonic bath for 5 min, and finally washed by distilled water.

(2) Pd layers were then electrodeposited on the surfaces of ZnO NRAs in aqueous solution of 0.002 M $PdCl_2$ + 0.0025 M sodium citrate by galvanostatic method at 1.0 mA/cm^2 for 15 min at 25 °C, and accordingly Pd/ZnO NRAs were fabricated. Then, PANI layers were further electrodeposited on the surfaces of Pd/ZnO NRAs in a solution of 0.1 M aniline + 0.1 M Na_2SO_4 by galvanostatic method at 1.5 mA/cm^2 for 5 min at 70 °C, and the PANI/Pd/ZnO NRAs were fabricated. After that, Pd layers were further electrodeposited on the surfaces of PANI/Pd/ZnO NRAs in aqueous solution of 0.002 M $PdCl_2$ + 0.0025 M sodium citrate by galvanostatic method at 1.0 mA/cm^2 for 15 min at 25 °C, and the Pd/PANI/Pd/ZnO four-layered NRAs were obtained.

(3) The Pd/PANI/Pd/ZnO four-layered NRAs were put into 3.0 M NaOH solution for 3 h to remove ZnO nanorods, and finally the Pd/PANI/Pd sandwich-structured nanotube arrays (SNTAs) were fabricated.

Structural Characterization. Surface morphologies of the Pd/PANI/Pd SNTAs were characterized by field emission scanning electron microscope (SEM, FEI, Quanta 400). Transmission electron microscope (TEM, JEM-2010HR), high resolution TEM (HRTEM, 200 kV), and electron diffraction (ED) were also used to characterize the microstructures of the products. The obtained products were also analyzed by X-ray diffraction (XRD, Bruker, D8 Advance) to determine the phases and structures. Chemical-state analysis of Pd in the fabricated Pd/PANI/Pd SNTAs was carried out by X-ray photoelectron spectroscopy (XPS) using an ESCALAB 250 X-ray photoelectron spectrometer. All XPS spectra were corrected using the C 1s line at 284.6 eV, and curve fitting and background subtraction were accomplished. The fabricated Pd/PANI/Pd SNTAs were also characterized by Fourier transform infrared spectroscopy (FTIR, Nicolet 330) and Raman spectroscopy (Renishaw inVia).

dx.doi.org/10.1021/ja403101r | J. Am. Chem. Soc. 2013, 135, 10703–10709

Electrochemical Characterization. The electrochemical properties of the prepared electrocatalysts were studied in a standard three-electrode electrolytic cell. A Pt foil served as the counter electrode. A saturated calomel electrode (SCE) with a double salt bridge system was utilized as the reference electrode that was connected to the cell. All potentials utilized in electrodeposition were the values vs SCE. The commercial Pd/C catalysts (Johnson Matthey, 20% Pd/C, Vulcan XC-72, Pd nanoparticle size 4 nm) are utilized in this study. The Pd/PANI/Pd SNTAs, Pd NTAs, and Pd/C catalysts all were loaded on the current collectors (Ti sheet, 1.0 cm^2) and then were served as a working electrode, respectively. The Pd loadings of Pd/PANI/Pd SNTAs, Pd NTAs, and commercial Pd/C catalysts are 105, 61, and 28 $\mu g/cm^2$, respectively. Cyclic voltammetry and chronoamperometry measurements were carried out on a CHI 660D electrochemical workstation (CH instruments, Inc.). Before the electrochemical measurements, the surfaces of electrocatalysts were covered by 10 μL Nafion (5 wt %) solution. Cyclic voltammograms (CVs) for ethanol electrooxidation were recorded between −0.80 and 0.20 V vs SCE at a scan rate of 50 mV/s. Chronoamperometry curves for ethanol electrooxidation were measured at −0.25 V. For the CV and chronoamperometry measurements of ethanol oxidation reactions, an aqueous solution of 1.0 M ethanol + 1.0 M NaOH was utilized in this study. Prior to all the experiments, the electrolyte solution was purged with high purity Ar gas for 10 min. All electrochemical measurements were carried out at 25 °C.

3. RESULTS AND DISCUSSION

The details of the fabrication are described in the Experimental Section in this paper. Figure 1a–e shows the schematic illustration of the procedures used to fabricate the Pd/PANI/Pd SNTAs. SEM images of the synthesized ZnO, Pd/ZnO, PANI/Pd/ZnO, and Pd/PANI/Pd/ZnO NRAs are shown in Figure S1a, S1b, S1c, and S1d in Supporting Information, respectively. It can be clearly seen that the Pd and PANI wraps favorably share the surfaces of ZnO nanorods and no deposit is packed into the interspaces of the nanorods. After dissolving ZnO, the Pd/PANI/Pd SNTAs are fabricated and their typical SEM image is shown in Figure 2a, which shows the Pd/PANI/Pd nanotubes have lengths of about 2 μm and are separate from each other. The inner diameters and wall thicknesses of Pd/PANI/Pd nanotubes are ∼300 and 50 nm, respectively. The high void volume is clearly seen in the Pd/PANI/Pd SNTAs and it will provide a three-dimensional (3D) space for mass transfer of reactant and resultant molecules. A typical transmission electron microscopy (TEM) image is shown in Figure 2b, which shows the Pd/PANI/Pd SNTAs have homogeneous wall thickness of about 50 nm. Pd nanoparticles uniformly distribute on the outer and inner surfaces of PANI nanotubes as shown in inset in Figure 2b. To demonstrate the sandwich-like structures, a TEM image of a broken Pd/PANI/Pd nanotube is measured and it is shown in Figure 2c, which clearly shows Pd nanoparticles uniformly disperse on the inner and outer surfaces of PANI layers, indicating the successful fabrication of the Pd/PANI/Pd SNTAs. The magnified TEM images of the outer and inner surfaces of PANI nanotubes are shown in Figure 2d and e, which further indicate that the Pd nanoparticles with sizes of 3–4 nm are uniformly dispersed. The thicknesses of outer Pd layer, middle PANI layer, and inner Pd layer in the sandwich structure are ∼14, ∼20, and ∼16 nm, respectively, as shown in Figure S2. The unique sandwich-like structures of the Pd/PANI/Pd SNTAs will allow the electroactive species to fully touch the catalysts and the Pd in Pd/PANI/Pd SNTAs to efficiently participate in the electrocatalytic reactions. HRTEM image and SAED pattern of Pd/PANI/Pd SNTAs were also measured, and the typical results are shown in Figure 2f, which shows the amorphous structures of Pd nanoparticles and PANI. XRD pattern of the Pd/PANI/Pd SNTAs is shown in Figure 3a, which shows no diffraction peak for Pd/PANI/Pd SNTAs besides the peaks of Ti substrate, further indicating the amorphous structure of Pd/PANI/Pd SNTAs. For the comparative study, here Pd

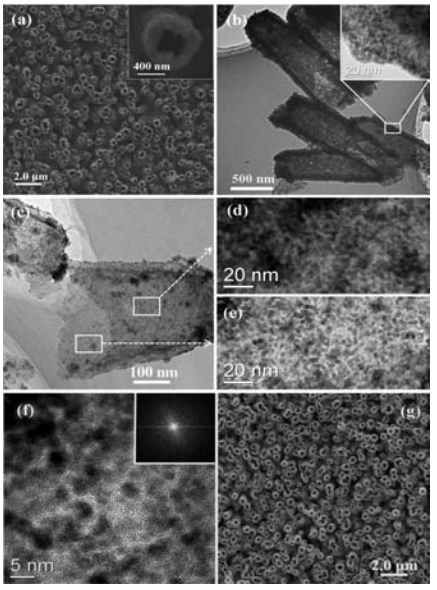

Figure 2. (a) SEM image of the Pd/PANI/Pd SNTAs. (b) TEM image of the Pd/PANI/Pd SNTAs. (c) TEM image of a broken Pd/PANI/Pd nanotube. (d) Magnified TEM image of the outer surface of the Pd/PANI/Pd nanotube. (e) Magnified TEM image of the inner surface of Pd/PANI/Pd nanotube. (f) HRTEM image and SAED pattern of the outer surface of Pd/PANI/Pd nanotube. (g) SEM image of Pd NTAs.

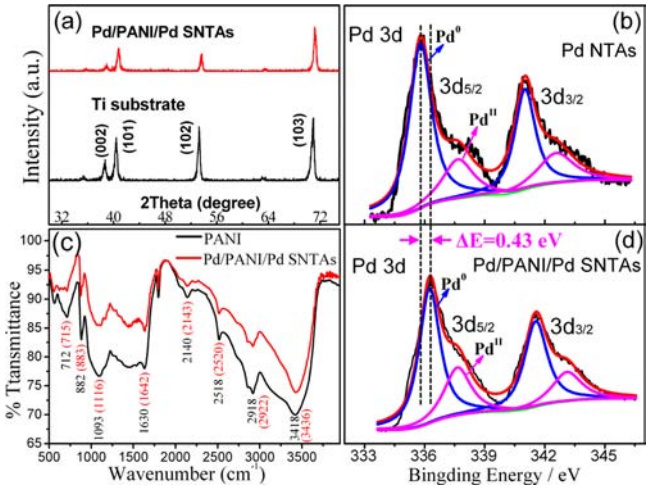

Figure 3. (a) XRD patterns of Pd/PANI/Pd SNTAs and Ti substrate. (b) XPS spectra of Pd 3d performed on Pd NTAs. (c) FT-IR spectra of PANI and Pd/PANI/Pd SNTAs. (d) XPS spectra of Pd 3d performed on Pd/PANI/Pd SNTAs.

dx.doi.org/10.1021/ja403101r | J. Am. Chem. Soc. 2013, 135, 10703–10709

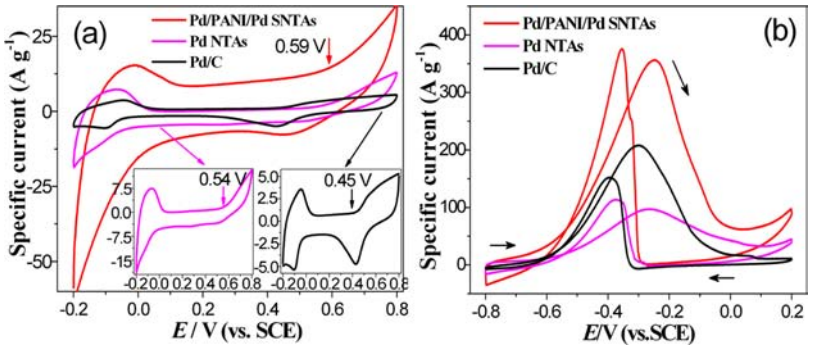

Figure 4. (a) CVs of the Pd/PANI/Pd SNTAs, Pd NTAs, and Pd/C catalysts measured in solution of 1.0 M H_2SO_4. (The inset at right in (a) is the magnified CV of Pd/C catalyst and the inset at left in (a) is the magnified CV of Pd NTAs.) (b) CVs of the Pd/PANI/Pd SNTAs, Pd NTAs, and Pd/C catalysts measured in solution of 1.0 M ethanol + 1.0 M NaOH at 50 mV/s.

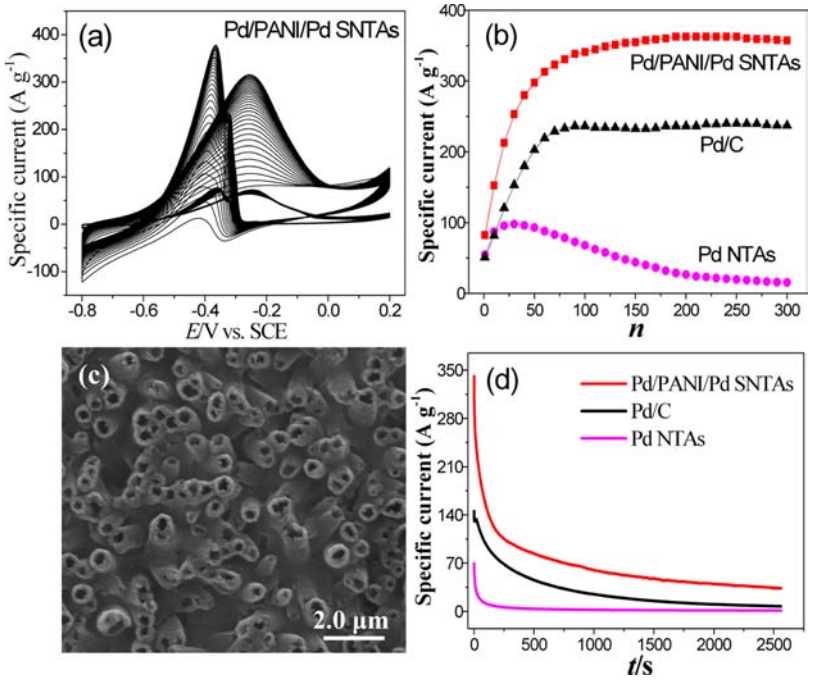

Figure 5. (a) CVs of Pd/PANI/Pd SNTAs from first to 300th cycle in solution of 1.0 M ethanol + 1.0 M NaOH at 50 mV/s. (b) Changes of the specific peak current densities of Pd/PANI/Pd SNTAs, Pd NTAs, and Pd/C catalysts with increasing cycle number. (c) SEM image of Pd/PANI/Pd SNTAs after 300 cycles. (d) Chronoamperometry curves of Pd/PANI/Pd SNTAs, Pd NTAs, and Pd/C catalysts measured in solution of 1.0 M ethanol + 1.0 M NaOH at 50 mV/s.

nanotube arrays (NTAs) were also synthesized by the similar route and their SEM image is shown in Figure 2g.

To prove the existence of Pd and investigate the effect of PANI on the electron structure of Pd, XPS spectra of Pd/PANI/Pd SNTAs and Pd NTAs in Pd 3d regions were measured as shown in Figure 3b and d, respectively. Each Pd 3d peak can be deconvoluted into two pairs of doublets. A comparison of the relative areas of integrated intensity of Pd^0 and Pd^{II} shows that the Pd mainly exists as Pd^0 in the Pd/PANI/Pd SNTAs and Pd NTAs. In addition, Figure 3b and d shows that the Pd $3d_{5/2}$ and $3d_{3/2}$ peaks of Pd/PANI/Pd SNTAs both shift to higher binding energies (336.23 and 341.56 eV) relative to the Pd $3d_{5/2}$ and $3d_{3/2}$ peaks of Pd NTAs (335.80 and 341.13 eV). The positive shifts (~0.43 eV) of Pd peaks in binding energies confirm the strong electron interactions involving Pd and PANI in the Pd/PANI/Pd SNTAs. The electron interactions between Pd and PANI obviously alter the electronic states of Pd atoms and accordingly will improve the catalytic activity and durability of Pd/PANI/Pd SNTAs.

To prove the existence of the PANI in Pd/PANI/Pd SNTAs and further investigate the electron interactions between Pd and PANI, Fourier transform IR spectroscopy (FT-IR) spectra of Pd/PANI/Pd SNTAs and PANI films were measured as shown in Figure 3c. Compared with the results in Figure 3c, the differences in FT-IR spectra of Pd/PANI/Pd SNTAs and PANI films are the shift in characteristic bands to slightly higher wavenumbers, such as the band in the marked area shifting from 3418 to 3436 cm^{-1}, and weaker peak intensities in the spectrum of Pd/PANI/Pd SNTAs. So, this result proves the existence of PANI in Pd/PANI/Pd SNTAs and also suggests the existence of strong electron interactions between the PANI layers and Pd nanoparticles.[61] In addition, the results of Raman and UV spectra of the Pd/PANI/Pd SNTAs and PANI films shown in Figure S4 also support the electron interactions between Pd and PANI in the Pd/PANI/Pd SNTAs.

dx.doi.org/10.1021/ja403101r | J. Am. Chem. Soc. 2013, 135, 10703−10709

Electrochemically active surface areas (EASAs) of the Pd/PANI/Pd SNTAs versus Pd NTAs and commercial Pd/C catalysts were analyzed basing on hydrogen desorption via cyclic voltammetry measurements (TEM image of the Pd/C catalyst is shown in Figure S5a). Figure 4a shows CVs of Pd/PANI/Pd SNTAs, Pd NTAs, and Pd/C catalysts in the deaerated H_2SO_4 solution (1.0 M) at 50 mV/s. Compared with Pd NTAs and Pd/C catalysts, the Pd/PANI/Pd SNTAs exhibit much larger specific desorption peaks, indicating much larger EASA of Pd/PANI/Pd SNTAs. The above results indicate that a higher proportion of Pd is electrochemically available in the Pd/PANI/Pd SNTAs than in Pd NTAs and Pd/C catalysts, and accordingly such Pd/PANI/Pd SNTAs can largely enhance the electroactive sites of catalysts. The ECSA enhancement of Pd/PANI/Pd SNTAs may be ascribed to the effect of PANI on electronic state of Pd, high content of metallic Pd, and highly uniform dispersion of Pd nanoparticles in the Pd/PANI/Pd SNTAs. In addition, the nanotube array structure of Pd/PANI/Pd SNTAs can highly improve the utilization rate of catalysts and the diffusion of electroactive species.

The electrocatalytic activity of Pd/PANI/Pd SNTAs toward ethanol oxidation along with Pd NTAs and Pd/C catalysts was investigated in solution of 1.0 M ethanol + 1.0 M NaOH. The CVs at 50 mV s^{-1} shown in Figure 4b show the specific peak current density of Pd/PANI/Pd SNTAs is almost 3.6 times and 1.7 times higher than those of Pd NTAs and Pd/C catalysts (the current densities all are normalized to the mass of Pd in catalysts), respectively, indicating the specific catalytic activity of the Pd/PANI/Pd SNTAs is much higher than those of Pd NTAs and Pd/C catalysts. In addition, the onset potential of forward anodic peak of the Pd/PANI/Pd SNTAs is obviously lower than those of Pd NTAs and Pd/C catalysts, indicating it is much more favorable for ethanol electrooxidation on the Pd/PANI/Pd SNTAs. Considering the similar surface morphology and the identical synthetic method, the much higher mass electrocatalytic activity of Pd/PANI/Pd SNTAs than that of Pd NTAs can be mainly ascribed to much larger ECSA and the synergetic effects between Pd and PANI. We also compared the surface area normalized activity (mA/cm^2 Pd) based on the electrochemical surface area of Pd, as shown in Figure S6. Compared with Pd NTAs, the Pd/PANI/Pd catalysts also show much higher surface area normalized activity.

Figure 5a shows CVs of Pd/PANI/Pd SNTAs with increasing cycle number, and the corresponding change of peak current density is shown in Figure 5b. The catalytic activity of Pd/PANI/Pd SNTAs has a drastic increase in the initial cycles and the maximum peak current density appears at about the 150th cycle. After 150 cycles, the peak current density almost remains stable with increasing cycle number, indicating long-term cycle stability for ethanol electrooxidation. In addition, Figure 5b shows that Pd/PANI/Pd SNTAs exhibit greatly enhanced catalytic activity and durability compared with Pd NTAs and Pd/C catalysts. After 300 cycles, the morphologies of Pd/PANI/Pd SNTAs still are maintained very well as shown in Figure 5c, indicating the high stability of Pd/PANI/Pd SNTAs.

The above results demonstrate the high electrocatalytic activity and durability of Pd/PANI/Pd SNTAs, and as electrocatalysts the Pd/PANI/Pd SNTAs show the following advantages as shown in Figure 1f: (*i*) The unique Pd/PANI/Pd SNTAs would relax transport of active species because of hollow nanotube array structures. (*ii*) The double thin layers of Pd in the SNTAs would enable fast electrochemical reactions and provide short diffusion paths for electroactive species. (*iii*) The SNTAs with double Pd shells would obviously enhance the utilization rate of Pd because of the anisotropic morphology, large specific surface area, and hollow nanostructures, and would efficiently prevent the Ostwald ripening and aggregation of catalysts during fuel cell operation. (*iv*) The Pd/PANI/Pd SNTAs directly grown on conductive substrate have an excellent electrical contact with current collectors, and this would allow each Pd/PANI/Pd nanotube to effectively participate in electrochemical reactions with almost no "dead" volume. Therefore, all of the above morphological merits highly promote the electrocatalytic activity and durability of Pd/PANI/Pd SNTAs together. In addition, the high activity and long-term durability of Pd/PANI/Pd SNTAs are especially attributed to the electron delocalization between Pd d orbitals and PANI π-conjugated ligands and to partial ionization due to electron transfer from Pd to PANI. The electron delocalization between Pd and PANI alters the electronic structure of Pd, making it difficult for metallic Pd to be oxidized (or dissolved) and accordingly enhancing the activity and durability of Pd/PANI/Pd SNTAs. The XPS results in Figure 3b and d demonstrate the shift of binding energies of Pd 3d of the Pd/PANI/Pd SNTAs. Prevention of the oxidation (or dissolution) of Pd in the Pd/PANI/Pd SNTAs can be further discerned in the CVs of Pd/PANI/Pd SNTAs, Pd NTAs, and Pd/C catalysts in 1.0 M H_2SO_4 as shown in Figure 4a. The onset potential of Pd oxidation of the Pd/PANI/Pd SNTAs catalyst is about 0.59 V, which is more positive than 0.54 V of Pd NTAs and 0.45 V of Pd/C catalysts. This result indicates that the oxidation of Pd in the Pd/PANI/Pd SNTAs is more difficult. In addition, the CVs of Pd/PANI/Pd SNTAs, Pd NTAs, and Pd/C catalysts were also measured in solution of 1.0 M NaOH as shown in Figure S7, which shows the onset potential of Pd oxidation of Pd/PANI/Pd SNTAs catalyst is much more positive than those of Pd NTAs and Pd/C catalysts. Therefore, the electron interactions between PANI and Pd can efficiently prevent the oxidation of Pd in Pd/PANI/Pd SNTAs and accordingly lead to greatly enhanced electroactivity and durability of the Pd/PANI/Pd SNTAs.[62]

To further evaluate the positive role of PANI in resisting surface poisoning of electrocatalysts, the chronoamperometry curves of Pd/PANI/Pd SNTAs, Pd NTAs, and Pd/C catalysts were also measured in solution of 1.0 M ethanol + 1.0 M NaOH as shown in Figure 5d. The potential was held at −0.25 V during the measurements. It is obvious that the Pd/PANI/Pd SNTAs exhibit a slower current decay over time in comparison with Pd NTAs and Pd/C catalysts, indicating a higher tolerance of Pd/PANI/Pd SNTAs to carbonaceous species generated during ethanol oxidation. In addition, Figure 5d shows the Pd/PANI/Pd SNTAs exhibit much higher current densities than Pd NTAs and Pd/C catalysts at all times, indicating that the Pd/PANI/Pd SNTAs have much higher electroactivity for ethanol oxidation than Pd NTAs and Pd/C catalysts. Therefore, the above results further demonstrate that the PANI layers can significantly improve the electrocatalytic activity and durability of Pd catalysts.

Here, high ability of CO antipoisoning of Pd/PANI/Pd SNTAs was also demonstrated. The catalytic activity of Pd/PANI/Pd SNTAs toward CO oxidation was contrasted with Pd NTAs and Pd/C catalysts in solution of 1.0 M NaOH at room temperature. In order to achieve the maximum coverage of CO at the Pd centers, high purity CO was bubbled into the electrolyte solution for 15 min while keeping the electrode

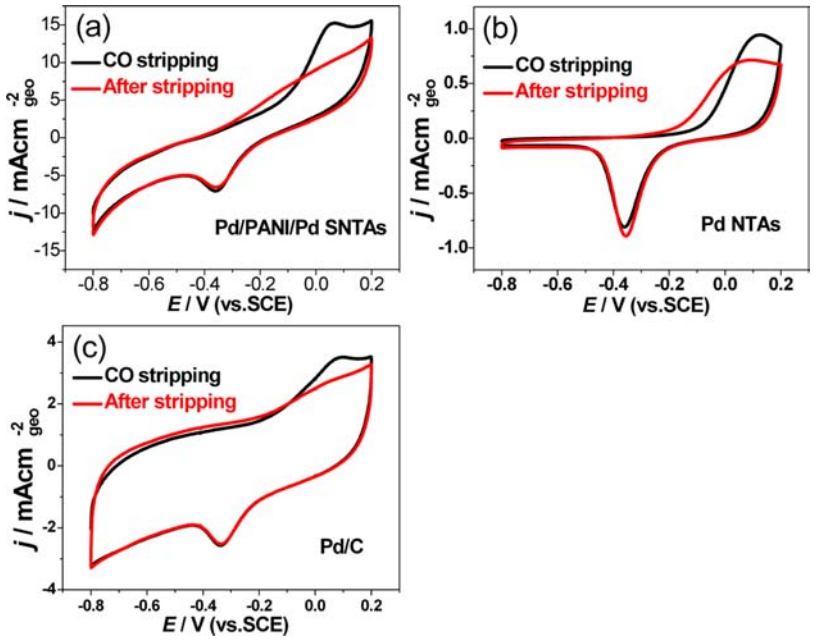

Figure 6. CO stripping measurements of (a) Pd/PANI/Pd SNTAs, (b) Pd NTAs, and (c) Pd/C catalysts performed in solution of 1.0 M NaOH at 50 mV s^{-1}.

potential at 0 V. Subsequently, the dissolved CO was purged out of electrolyte by bubbling Ar gas for 20 min. Figure 6 shows two consecutive CVs of Pd/PANI/Pd SNTAs, Pd NTAs, and Pd/C catalysts recorded between −0.8 and 0.2 V at 50 mV s^{-1} in CO saturated solution of 1.0 M NaOH. In the initial forward scan of CO stripping, a much larger CO oxidation peak is clearly seen on Pd/PANI/Pd SNTAs compared with Pd NTAs and Pd/C catalysts, which could be attributed to much larger ECSA of Pd/PANI/Pd SNTAs. In addition, in the initial forward scan of CO stripping, the onset potential (−0.2 V) of CO oxidation on Pd/PANI/Pd SNTAs is obviously more negative than those on Pd NTAs (−0.10 V) and Pd/C catalysts (−0.16 V). This result indicates that the PANI in the Pd/PANI/Pd SNTAs can facilitate removal of CO from the surface of Pd. In addition, the disappearance of CO oxidation peaks after stripping also indicates the Pd/PANI/Pd SNTAs are free of dissolved CO.

4. CONCLUSIONS

In conclusion, the novel Pd/PANI/Pd SNTAs were successfully fabricated via template-assisted electrodeposition that is a facile and high efficiency method. The unique SNTAs structures provide the fast transport and short diffusion paths for electroactive species and accordingly fast electrochemical reactions for ethanol oxidation because of the hollow nanotubes, sandwich-like structures, and array structures. In addition, the Pd/PANI/Pd SNTAs with double Pd shells would obviously enhance the utilization rate of Pd and would efficiently prevent the Ostwald ripening and aggregation of catalysts. The experimental results demonstrate that these Pd/PANI/Pd SNTAs exhibit significantly improved catalytic activity and durability compared with Pd NTAs and Pd/C catalysts. Besides the nanotube array structure, the improved activity and durability are especially attributed to the novel Pd/PANI/Pd sandwich-like structure, which results in electron delocalization between Pd d orbitals and PANI π-conjugated ligands and in electron transfer from Pd to PANI. Here the certified perfect inosculation of compositionally and geometrically favorable factors provides a novel design strategy to prepare electrocatalysts with excellent electroactivity and durability.

■ ASSOCIATED CONTENT

Ⓢ Supporting Information

SEM images, TEM images, EDS spectrum, Raman spectra, and CVs. This material is available free of charge via the Internet at http://pubs.acs.org.

■ AUTHOR INFORMATION

Corresponding Author

*E-mail: ligaoren@mail.sysu.edu.cn

Notes

The authors declare no competing financial interest.

■ ACKNOWLEDGMENTS

This work was supported by NSFC (51173212, 21073240, and 21273290), Fundamental Research Fund for the Central Universities (13lgpy51), Research Fund for New Star Scientist of Pearl River Science and Technology of Guangzhou (2011J2200057), Research Fund for the Doctoral Program of Higher Education of China (No. 20120171110043), SRF for ROCS, SEM ([2012]1707), and Open-End Fund of State Key Lab of Physical Chemistry of Solid Surfaces of Xiamen University (201113).

■ REFERENCES

(1) Greeley, J.; Stephens, I. E. L.; Bondarenko, A. S.; Johansson, T. P.; Hansen, H. A.; Jaramillo, T. F.; Rossmeisl, J.; Chorkendorff, I.; Nørskov, J. K. *Nature Chem.* **2009**, *1*, 552−556.

(2) Xia, B. Y.; Wu, H. B.; Wang, X.; Lou, X. W. *J. Am. Chem. Soc.* **2012**, *134*, 13934−13937.

(3) Wu, J.; Qi, L.; You, H.; Gross, A.; Li, J.; Yang, H. *J. Am. Chem. Soc.* **2012**, *134*, 11880−11883.

(4) Wang, H.; Ishihara, S.; Ariga, K.; Yamauchi, Y. *J. Am. Chem. Soc.* **2012**, *134*, 10819−10821.

(5) Wang, D.-Y.; Chou, H.-L.; Lin, Y.-C.; Lai, F.-J.; Chen, C.-H.; Lee, J.-F.; Hwang, B.-J.; Chen, C.-C. *J. Am. Chem. Soc.* **2012**, *134*, 10011−10020.
(6) Ma, X.; Meng, H.; Cai, M.; Shen, P. K. *J. Am. Chem. Soc.* **2012**, *134*, 1954−1957.
(7) Strmcnik, D.; Kodama, K.; van der Vliet, D.; Greeley, J.; Stamenkovic, V.; Marković, N. M. *Nat. Chem.* **2009**, *1*, 466−472.
(8) Debe, M. K. *Nature* **2012**, *486*, 43−51.
(9) Yamamoto, K.; Imaoka, T.; Chun, W.-J.; Enoki, O.; Katoh, H.; Takenaga, M.; Sonoi, A. *Nat. Chem.* **2009**, *1*, 397−402.
(10) Strmcnik, D.; Escudero-Escribano, M.; Kodama, K.; Stamenkovic, V. R.; Cuesta, A.; Marković, N. M. *Nat. Chem.* **2010**, *2*, 880−885.
(11) Stamenkovic, V. R.; Mun, B. S.; Arenz, M.; Mayrhofer, K. J. J.; Lucas, C. A.; Wang, G.; Ross, P. N.; Markovic, N. M. *Nat. Mater.* **2007**, *6*, 241−247.
(12) Kibsgaard, J.; Chen, Z.; Reinecke, B. N.; Jaramillo, T. F. *Nat. Mater.* **2012**, *11*, 963−969.
(13) Li, Y.; Zhou, W.; Wang, H.; Xie, L.; Liang, Y.; Wei, F.; Idrobo, J.-C.; Pennycook, S. J.; Dai, H. *Nat. Nanotechnol.* **2012**, *7*, 394−400.
(14) Suntivich, J.; Gasteiger, A.; Yabuuchi, N.; Nakanishi, H.; Goodenough, J. B.; Shao-Horn, Y. *Nat. Chem.* **2011**, *3*, 546−550.
(15) Cheng, F.; Shen, J.; Peng, B.; Pan, Y.; Tao, Z.; Chen, J. *Nat. Chem.* **2010**, *3*, 79−84.
(16) Liu, W.; Herrmann, K.; Geiger, D.; Borchardt, L.; Simon, F.; Kaskel, S.; Gaponik, N.; Eychmüller, A. *Angew. Chem., Int. Ed.* **2012**, *51*, 5743−5746.
(17) Huang, X.; Zhang, H.; Guo, C.; Zhou, Z.; Zheng, N. *Angew. Chem., Int. Ed.* **2009**, *48*, 4808−4812.
(18) Mazumder, V.; Chi, M.; Mankin, M.; Liu, Y.; Metin, O.; Sun, D.; More, K. L.; Sun, S. *Nano Lett.* **2012**, *12*, 1102−1106.
(19) Jin, M.; Zhang, H.; Xie, Z.; Xia, Y. *Angew. Chem., Int. Ed.* **2011**, *50*, 7850−7854.
(20) Wu, H.; Li, H.; Zhai, Y.; Xu, X.; Jin, Y. *Adv. Mater.* **2012**, *24*, 1594−1597.
(21) Yin, S.; Cai, M.; Wang, C.; Shen, P. K. *Energy Environ. Sci.* **2011**, *4*, 558−563.
(22) Huang, X.; Tang, S.; Mu, X.; Dai, Y.; Chen, G.; Zhou, Z.; Ruan, F.; Yang, Z.; Zheng, N. *Nat. Nanotechnol.* **2011**, *6*, 28−32.
(23) Xu, J.; Wilson, A. R.; Rathmell, A. R.; Howe, J.; Chi, M.; Wiley, B. J. *ACS Nano* **2011**, *5*, 6119−6127.
(24) Wang, L.; Nemoto, Y.; Yamauchi, Y. *J. Am. Chem. Soc.* **2011**, *133*, 9674−9677.
(25) Zhang, H.; Jin, M.; Wang, J.; Li, W.; Camargo, P. H. C.; Kim, M. J.; Yang, D.; Xie, Z.; Xia, Y. *J. Am. Chem. Soc.* **2011**, *133*, 6078−6089.
(26) Guo, S.; Dong, S.; Wang, E. *ACS Nano* **2010**, *4*, 547−555.
(27) Peng, Z.; Yang, H. *J. Am. Chem. Soc.* **2009**, *131*, 7542−7543.
(28) Shao, M.; Sasaki, K.; Adzic, R. R. *J. Am. Chem. Soc.* **2006**, *128*, 3526−3527.
(29) Yin, A.-X.; Min, X.; Zhang, Y.-W.; Yan, C.-H. *J. Am. Chem. Soc.* **2011**, *133*, 3816−3819.
(30) Hong, J. W.; Kim, D.; Lee, Y. W.; Kim, M.; Kang, S. W.; Han, S. W. *Angew. Chem., Int. Ed.* **2011**, *50*, 8876−8880.
(31) Baber, A. E.; Tierney, H. L.; Sykes, E. C. H. *ACS Nano* **2010**, *4*, 1637−1645.
(32) Lee, Y. W.; Kim, M.; Kang, S. W.; Han, S. W. *Angew. Chem., Int. Ed.* **2011**, *50*, 3466−3470.
(33) Markovic, N. M. *Nat. Mater.* **2013**, *12*, 101−102.
(34) Tian, N.; Zhou, Z.; Yu, N.-F.; Wang, L.-Y.; Sun, S.-G. *J. Am. Chem. Soc.* **2010**, *132*, 7580−7581.
(35) Liang, H.-W.; Liu, S.; Gong, J.; Wang, S.; Wang, L.; Yu, S.-H. *Adv. Mater.* **2009**, *21*, 1850−1854.
(36) Chen, Z.; Waje, M.; Li, W.; Yan, Y. *Angew. Chem., Int. Ed.* **2007**, *46*, 4060−4063.
(37) Cui, C.-H.; Li, H.-H.; Yu, J.-W.; Gao, M.-R.; Yu, S.-H. *Angew. Chem., Int. Ed.* **2010**, *49*, 9149−9152.
(38) Koenigsmann, C.; Santulli, A. C.; Gong, K.; Vukmirovic, M. B.; Zhou, W.; Sutter, E.; Wong, S. S.; Adzic, R. R. *J. Am. Chem. Soc.* **2011**, *133*, 9783−9795.
(39) Yin, A.-X.; Min, X.-Q.; Zhu, W.; Wu, H.-S.; Zhang, Y.-W.; Yan, C.-H. *Chem. Commun.* **2012**, *48*, 543−545.
(40) Guo, S.; Dong, S.; Wang, E. *Energy Environ. Sci.* **2010**, *3*, 1307−1310.
(41) Kim, D.; Lee, Y. W.; Lee, S. B.; Han, S. W. *Angew. Chem., Int. Ed.* **2012**, *51*, 159−163.
(42) Lu, C.-L.; Prasad, K. S.; Wu, H.-L.; Ho, J. A.; Huang, M. H. *J. Am. Chem. Soc.* **2010**, *132*, 14546−14553.
(43) Shao, M.; Shoemaker, K.; Peles, A.; Kaneko, K.; Protsailo, L. *J. Am. Chem. Soc.* **2010**, *132*, 9253−9255.
(44) Mayrhofer, K.J. J.; Hartl, K.; Juhart, V.; Arenz, M. *J. Am. Chem. Soc.* **2009**, *131*, 16348−16349.
(45) Ji, X.; Lee, K. T.; Holden, R.; Zhang, L.; Zhang, J.; Botton, G.; Couillard, M.; Nazar, L. F. *Nat. Chem.* **2010**, *2*, 286−293.
(46) Li, Y.; Li, Y.; Zhu, E.; McLouth, T.; Chiu, C.-Y.; Huang, X.; Huang, Y. *J. Am. Chem. Soc.* **2012**, *134*, 12326−12329.
(47) Kinoshita, K. *Carbon: Electrochemical and Physicochemical Properties*; Wiley: New York, 1988; p 319.
(48) Koenigsmann, C.; Zhou, W.; Adzic, R. R.; Sutter, E.; Wong, S. S. *Nano Lett.* **2010**, *10*, 2806−2811.
(49) Wang, D.; Xin, H. L.; Hovden, R.; Wang, H.; Yu, Y.; Muller, D. A.; DiSalvo, F. J.; Abruña, H. D. *Nat. Mater.* **2012**, *11*, 81−87.
(50) Van der Vliet, D.; Wang, C.; Tripkovic, D.; Strmcnik, D.; Zhang, X. F.; Debe, M. K.; Atanasoski, R. T.; Markovic, N. M.; Stamenkovic, V. R. *Nat. Mater.* **2012**, *11*, 1051−1058.
(51) Zhou, H. J.; Zhou, W. P.; Adzic, R. R.; Wong, S. S. *J. Phys. Chem. C* **2009**, *113*, 5460−5466.
(52) Gao, W.; Sattayasamitsathit, S.; Orozco, J.; Wang, J. *J. Am. Chem. Soc.* **2011**, *133*, 11862−11864.
(53) He, D.; Zeng, C.; Xu, C.; Cheng, N.; Li, H.; Mu, S.; Pan, M. *Langmuir* **2011**, *27*, 5582−5588.
(54) Shi, L.; Liang, R.-P.; Qiu, J.-D. *J. Mater. Chem.* **2012**, *22*, 17196−17203.
(55) Guo, S.; Dong, S.; Wang, E. *Small* **2009**, *5*, 1869−1876.
(56) Salavagione, H J.; Sanchís, C.; Morallón, E. *J. Phys. Chem. C* **2007**, *111*, 12454−12460.
(57) Chen, S.; Wei, Z. D.; Qi, X.; Dong, L.; Guo, Y.-G.; Wan, L.-J.; Shao, Z.; Li, L. *J. Am. Chem. Soc.* **2012**, *134*, 13252−13255.
(58) Kowal, A.; Li, M.; Shao, M.; Sasaki, K.; Vukmirovic, M. B.; Zhang, J.; Marinkovic, N. S.; Liu, P.; Frenkel, A. I.; Adzic, R. R. *Nat. Mater.* **2009**, *8*, 325−330.
(59) Drelinkiewicz, A.; Hasik, M.; Kloc, M. *Synth. Met.* **1999**, *102*, 1307−1308.
(60) Gao, M.-R.; Gao, Q.; Jiang, J.; Cui, C.-H.; Yao, W.-T.; Yu, S.-H. *Angew. Chem., Int. Ed.* **2011**, *50*, 4905−4908.
(61) Liu, L.; Pippel, E. *Angew. Chem., Int. Ed.* **2011**, *50*, 2729−2733.
(62) Pandey, R. K.; Lakshminarayanan, V. *J. Phys. Chem. C* **2009**, *113*, 21596−21603.